Barriers and Deformation in Fission of Charged Metal Clusters

C. Yannouleas* and Uzi Landman

School of Physics, Georgia Institute of Technology, Atlanta, Georgia 30332-0430

Received: June 6, 1995[⊗]

The influence of electronic shell effects on the barriers and channels pertaining to metal-cluster fission is studied using a shell correction method in connection with an asymmetric two-center-oscillator model potential. This approach has the advantage that the ensuing shape parametrization allows for an independent variation of the deformations of parent and daughter clusters. Results for both symmetric and asymmetric channels associated with the parent clusters Na_{10}^{2+} and Na_{18}^{2+} are presented. We find that barriers, which separate the parent configuration from molecular-type configurations associated with preformation of the fragments, are most important and must be considered, together with the subsequent separation process, for proper elucidation of metal-cluster fission phenomena.

Introduction

Charged metal clusters break up into smaller fragments[1−4] when the accumulation of excess charges on them (caused by successive ionizations) reaches beyond the point at which the repulsive Coulomb forces can overcome the electronic binding. Such a fragmentation process is usually referred to as cluster fission and bears certain analogies to the well-known and rather well-understood processes[5] of nuclear fission and α-radioactivity, despite the differences in the nature of binding in nuclei and in metallic clusters and the vast disparities in the spatial and temporal scales characterizing these systems. Consequently, the extension of theoretical ideas and models formulated in the context of nuclear fission and α-radioactivity and their adaptation to the process of fission in clusters appears as a promising avenue of research.

The main aim of the present paper is to study the influence of electronic shell effects on barriers and channels pertaining to metal-cluster fission. Such effects are essential in describing the details of nuclear fission in symmetric and moderately asymmetric cases. As we will elaborate below, they are also essential in the case of small metal clusters, since the existence and magnitude of a fission barrier may depend exclusively on such effects. In particular, unlike the nuclear case of α-radioactivity, the importance of electronic shell effects for metal-cluster fission may not diminish even for superasymmetric channels (e.g., those emitting a trimer cation). This behavior arises from the fact that preformation-type Coulombic barriers (familiar from α-decay) are rather weak in metal clusters due to small relative magnitude of the surface tension and to small values of the total charge as compared to the nuclear case. As we will see in this study, this is particularly true for doubly charged clusters, which constitute the majority of cases studied to date experimentally.[1,2,4]

The method we adopt for studying metal-cluster fission is a generalization of the semiempirical shell correction method (SE-SCM) of ref 6, which has provided an excellent description of ground-state properties of simple metal clusters (Na_N, K_N, Cu_N) when the triaxial degree of deformation is considered[7] (partial results of our SE-SCM method for metal-cluster fission have been presented in ref 8, which focused on the physical principles underlying cluster fission in connection with investigations based on ab initio molecular dynamics calculations[9,4] and existing analogies with nuclear phenomena of fission and exotic and α-radioactivity).

In the SE-SCM method, we need to introduce appropriate model potentials. As will become apparent from our results, one-center potentials (like the one-center anisotropic harmonic oscillator of ref 6) are not adequate for describing shell effects in the fission of small metal clusters; rather, a two-center potential is required. Indeed, the model potentials should be able to simulate the fragmentation of the initial parent cluster toward a variety of asymptotic daughter-cluster shapes, e.g., two spheres in the case of double magic fragments, a sphere and a spheroid in the case of a single magic fragment or two spheroids in a more general case. In the case of metal clusters, asymmetric channels are most common, and thus a meaningful and flexible description of the asymmetry is of primary concern. We found that such a required degree of flexibility can be provided via the shape parametrization of the asymmetric two-center-oscillator shell model (ATCOSM) introduced earlier in nuclear fission.[10]

In addition to the present shape parametrization,[8] other two-center shape parametrizations [mainly in connection with Kohn−Sham local density functional (KS-LDA) jellium calculations] have been used[11−13] in studies of metal cluster fission. They can be grouped into two categories, namely, the two-intersected-spheres jellium,[11,14] and the variable-necking-in parametrizations.[12,13] In the latter group, ref 12 accounts for various necking-in situations by using the "funny-hills" parametrization,[15] while ref 13 describes the necking-in by connecting two spheres smoothly through a quadratic surface. The limitation of these other parametrizations is that they are not flexible enough to account for the majority of the effects generated by the shell structure of the parent and daughters, which in general have not spherical but deformed (independently from each other) shapes. An example is offered by the case of the parent Na_{18}^{2+}, which has a metastable oblate ground state and thus cannot be described by any one of the above parametrizations. We wish to emphasize again that one of the conclusions of the present work is that the shell structure of the (independently deformed) parent and daughters are the dominant factors specifying the fission barriers, and thus parametrizations[11−13] with restricted final fragments (or parent) shapes are deficient in accounting for some of the most important features governing metal-cluster fission.

[⊗] Abstract published in *Advance ACS Abstracts,* September 15, 1995.

0022-3654/95/2099-14577$09.00/0

Outline of Theoretical Method

In the ATCOSM approach, the single-particle levels, associated with both the initial one-fragment parent and the separated daughters emerging from cluster fission, are determined by the following single-particle Hamiltonian:[10,16]

$$H = T + {}^1/_2 m_e \omega_{\rho i}{}^2 \rho^2 + {}^1/_2 m_e \omega_{zi}{}^2 (z - z_i)^2 + V_{\text{neck}}(z) + U(\mathbf{l}_i{}^2) \tag{1}$$

where $i = 1$ for $z < 0$ (left) and $i = 2$ for $z > 0$ (right).

This Hamiltonian is axially symmetric along the z axis. ρ denotes the cylindrical coordinate perpendicular to the symmetry axis. The shapes described by this Hamiltonian are those of two semispheroids (either prolate or oblate) connected by a smooth neck [which is specified by the term $V_{\text{neck}}(z)$]. $z_1 < 0$ and $z_2 > 0$ are the centers of these semispheroids. For the smooth neck, the following fourth-order expression[16] was adopted, namely

$$V_{\text{neck}}(z) = {}^1/_2 m_e \xi_i \omega_{zi}{}^2 (z - z_i)^4 \theta(|z| - |z_i|) \tag{2}$$

where $\theta(x) = 0$ for $x > 0$ and $\theta(x) = 1$ for $x < 0$.

The frequency $\omega_{\rho i}$ in eq 1 must be z-dependent in order to interpolate smoothly between the values $\omega^\circ_{\rho i}$ of the lateral frequencies associated with the left ($i = 1$) and right ($i = 2$) semispheroids, which are not equal in asymmetric cases. The frequencies $\omega^\circ_{\rho i}$ ($i = 1, 2$) characterize the lateral harmonic potentials associated with the two semispheroids outside the neck region. In the implementation of such an interpolation, we follow ref 16.

The angular-momentum dependent term $U(\mathbf{l}_i{}^2)$, where $\mathbf{l}_1$ and $\mathbf{l}_2$ are pseudoangular momenta with respect to the left and right centers z_1 and z_2, is a direct generalization of the corresponding term familar from the one-center Nilsson potential (e.g., see ref 6). Its function is to lift the usual harmonic-oscillator degeneracies for different angular momenta, that is, for a spherical shape the 1d−2s degeneracy is properly lifted into a 1d shell that is lower than the 2s shell (for the parameters entering into this term, which ensure a proper transition from the case of the fissioning cluster to that of the separated two fragments, we have followed ref 16).

The cluster shapes associated with the spatial-coordinate-dependent single-particle potential $V(\rho,z)$ in the Hamiltonian (1) are determined by the assumption that the cluster surface coincides with an equipotential surface of value V_0, namely, from the relation $V(\rho,z) = V_0$. Subsequently, one solves for ρ and derives the cluster shape $\rho = \rho(z)$. For the proper value of V_0, we take the one associated with a spherical shape containing the same number of atoms, N_Z, as the parent cluster, namely, $V_0 = {}^1/_2 m_e \omega_0{}^2 R^2$, where $\hbar\omega_0 = 49 r_s{}^{-2} N_Z{}^{-1/3}$ eV, $R = r_s N_Z{}^{1/3}$, and r_s is the Wigner−Seitz radius. Volume conservation is implemented by requiring that the volume enclosed by the fissioning cluster surface (even after separation) remains equal to $4\pi R^3/3$.

The cluster shape in this parametrization is specified by four independent parameters. We take them to be as follows: the separation $d = z_2 - z_1$ of the semispheroids; the asymmetry ratio $q_{as} = \omega^\circ_{\rho 2}/\omega^\circ_{\rho 1}$; and the deformation ratios for the left (1) and right (2) semispheroids $q_i = \omega_{zi}/\omega^\circ_{\rho i}$ ($i = 1, 2$).

The single-particle levels of the Hamiltonian in eq 1 are obtained by numerical diagonalization in a basis consisting of the eigenstates of the following auxiliary Hamiltonian:

$$H_0 = T + {}^1/_2 m_e \bar{\omega}_\rho{}^2 \rho^2 + {}^1/_2 m_e \omega_{zi}{}^2 (z - z_i)^2 \tag{3}$$

where $\bar{\omega}_\rho$ is the arithmetic average of $\omega^\circ_{\rho 1}$ and $\omega^\circ_{\rho 2}$. The eigenvalue problem specified by the auxiliary Hamiltonian(3) is separable in the cylindrical variables ρ and z. The general solutions in ρ are those of a two-dimensional oscillator, while in z they can be expressed through the parabolic cylinder functions.[17] The matching conditions at $z = 0$ for the left and right domains yield the z eigenvalues and the associated eigenfunctions.[10]

Having obtained the single-particle spectra, the empirical shell correction (in the spirit of Strutinsky's method[18]), $\Delta E^{\text{Str}}_{\text{sh}}$, is determined from

$$\Delta E^{\text{Str}}_{\text{sh}} = \sum_i^{\text{occ}} \epsilon_i - E^{\text{Str}}_{\text{av}} \tag{4}$$

The single-particle average, $E^{\text{Str}}_{\text{av}}$, is calculated[19] through an $\hbar$ expansion of the semiclassical partition function introduced by Wigner and Kirkwood. For general-shape potentials, this last method amounts[19] to eliminating the semiclassical Fermi energy $\tilde{\lambda}$ from the set of the following two equations:

$$N_e = \frac{1}{3\pi^2}\left(\frac{2m_e}{\hbar^2}\right)^{3/2} \int^{\mathbf{r}_{\tilde{\lambda}}} d\mathbf{r} \left[(\tilde{\lambda} - V)^{3/2} - \frac{1}{16}\frac{\hbar^2}{2m_e}(\tilde{\lambda} - V)^{-1/2}\nabla^2 V\right] \tag{5}$$

$$E^{\text{Str}}_{\text{av}} = \frac{1}{3\pi^2}\left(\frac{2m_e}{\hbar^2}\right)^{3/2} \int^{\mathbf{r}_{\tilde{\lambda}}} d\mathbf{r} \left(\left[\frac{3}{5}(\tilde{\lambda} - V)^{5/2} + V(\tilde{\lambda} - V)^{3/2}\right] + \frac{1}{16}\frac{\hbar^2}{2m_e}[(\tilde{\lambda} - V)^{1/2}\nabla^2 V - V(\tilde{\lambda} - V)^{-1/2}\nabla^2 V]\right) \tag{6}$$

where N_e is the total number of delocalized valence electrons, and $V(\rho,z)$ is the potential in the single-particle Hamiltonian of eq 1. The domain of integration is demarcated by the classical turning point $\mathbf{r}_{\tilde{\lambda}}$, such that $V(\mathbf{r}_{\tilde{\lambda}}) = \tilde{\lambda}$.

Finally, from the liquid-drop-model (LDM) contributions (e.g., see refs 6 and 20), we retain the two most important ones, namely, the surface contribution and the Coulomb repulsion. To determine the surface contribution, we calculate numerically the area of the surface of the fissioning cluster shape, $\rho = \rho(z)$, and multiply it by a surface-tension coefficient specified via an extended Thomas−Fermi (ETF) LDA calculation for spherical jellia.[6,20−22] The Coulomb repulsion is calculated numerically using the assumption of a classical conductor (for a more elaborate application of the LDM to triaxially deformed ground states of neutral and charged metal clusters described via a one-center shape parametrization, see ref 6).

In brief, the total energy E_t is given by

$$E_t = E_{\text{LDM}} + \Delta E^{\text{Str}}_{\text{sh}} = E_S + E_C + \Delta E^{\text{Str}}_{\text{sh}} \tag{7}$$

where E_S and E_C are the surface and Coulomb terms, respectively.

Results

As a demonstration of our method, we present reults for two different parents, namely, $Na_{10}{}^{2+}$ and $Na_{18}{}^{2+}$. These choices allow us to study the influence of the shell effects, associated with a variety of combination of shapes for both parents and fragments, on the fission barriers. The case of $Na_{18}{}^{2+}$ also allows us to study the competition between two magic-number channels, namely, $Na_{18}{}^{2+} \rightarrow 2Na_9{}^+$ and $Na_{18}{}^{2+} \rightarrow Na_{15}{}^+ + Na_3{}^+$ (where $Na_9{}^+$ and $Na_3{}^+$, containing eight and two electrons, respectively, are the magic clusters). This case is particularly interesting, since from energetics arguments it is expected to

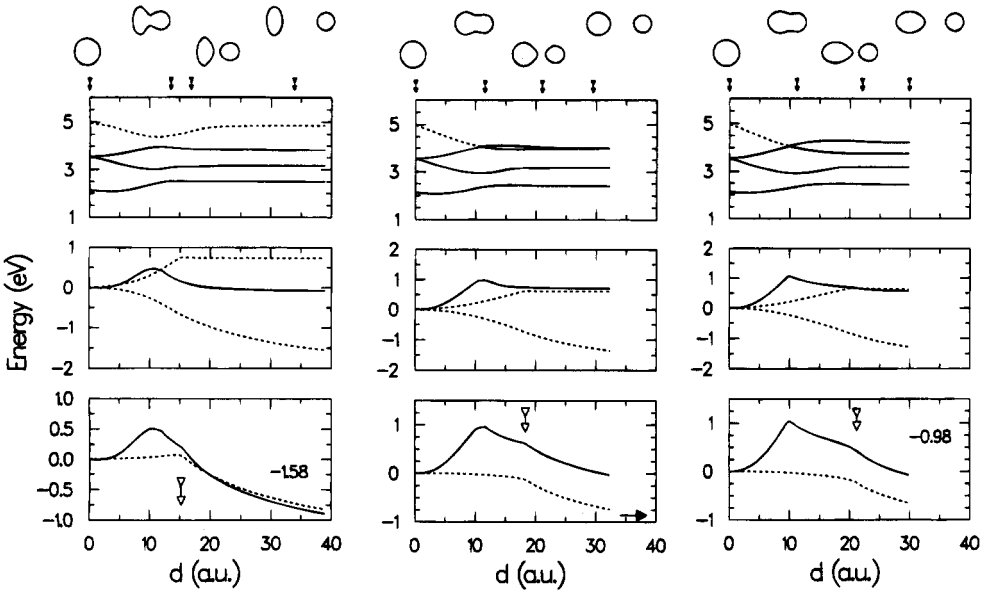

Figure 1. ATCOSM results for the asymmetric channel $Na_{10}^{2+} \rightarrow Na_7^+ + Na_3^+$. The final configuration of Na_3^+ is spherical. For the heavier fragment Na_7^+, we present results associated with three different final shape configurations, namely, oblate [(o, s); left], spherical [(s, s); middle], and prolate [(p, s); right]. The ratio of shorter over longer axis is 0.555 for the oblate case and 0.75 for the prolate case. Bottom: LDM energy (surface plus Coulomb, dashed curve) and total potential energy (LDM plus shell corrections, solid curve) as a function of fragment separation d. The empty vertical arrow marks the scission point. The zero of energy is taken at $d = 0$. A number (−1.58 or −0.98 eV), or a horizontal solid arrow, denotes the corresponding dissociation energy. Middle: Shell-correction contribution (solid curve), surface contribution (upper dashed curve), and Coulomb contribution (lower dashed curve) to the total energy, as a function of fragment separation d. Top: Single-particle spectra as a function of fragment separation d. The occupied (fully or partially) levels are denoted with solid lines. The unoccupied levels are denoted with dashed lines. On top of the figure, four snapshots of the evolving cluster shapes are displayed. The solid vertical arrows mark the corresponding fragment separations. Observe that the doorway molecular configurations correspond to the second snapshot from the left. Notice the change in energy scale for the middle and bottom panels, as one passes from (o, s) to (s, s) and (p, s) final configurations.

be the first instance where a magic fragment other than the trimer[9] becomes the favored channel.[2,6]

A. Closed-Shell Parent Na_{10}^{2+}. Figure 1 presents results for the channel $Na_{10}^{2+} \rightarrow Na_7^+ + Na_3^+$ for three different cases, namely, when the larger fragment, Na_7^+, is oblate (left column), spherical (middle column), and prolate (right column). From our one-center analysis, we find as expected that Na_7^+ (six electrons) has an oblate global minimum and a higher-in-energy prolate local minimum. In the two-center analysis, we have calculated the fission pathways so that the emerging fragments correspond to possible deformed one-center minima. It is apparent that the most favored channel (i.e., having the lowest barrier, see the solid line in the bottom panels) will yield an oblate Na_7^+ (left column in Figure 1), in agreement with the expectations from the one-center energetics analysis.

The middle panels exhibit the decomposition of the total barrier into the three components of surface, Coulomb, and shell-correction terms (see eq 7), which are denoted by an upper dashed curve, a lower dashed curve, and a solid line, respectively. The total LDM contribution (surface plus Coulomb) is also exhibited at the bottom panels (dashed lines).

It can be seen that the LDM barrier is either absent or very small and that the total barrier is due almost exclusively to electronic shell effects. The total barrier has a double-humped structure, with the outer hump corresponding to the LDM saddle point, which also happens to be the scission point (indicated by an empty vertical arrow). The inner hump coincides with the peak of the shell-effect term and is associated with the rearrangement of single-particle levels from the initial spherical parent to a molecular configuration resembling a Na_7^+ attached to a Na_3^+. Such molecular configurations (discovered earlier in ab initio molecular dynamics simulations[4,8,9] of the fission of charged metal clusters, as well as in studies of the fusion of neutral clusters[23]) are a natural precursor toward full fragment separation and complete fission, and naturally they give rise to the notion of preformation of the emerging fragments.[4,8,9]

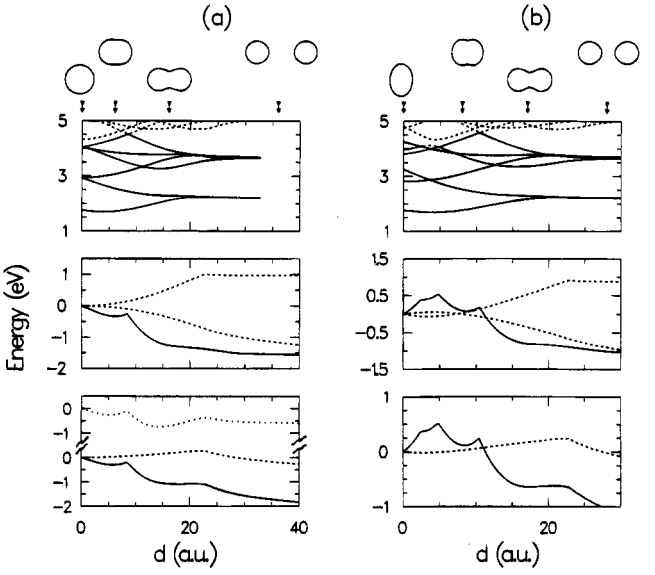

Figure 2. ATCOSM results for the symmetric channel $Na_{18}^{2+} \rightarrow 2Na_9^+$, when the initial parent shape is assumed (a) spherical and (b) oblate (with a shorter over longer axis ratio equal to 0.699). Panel distribution and other notations and conventions are the same as in Figure 1. The top dotted line in the bottom panel of (a) represents the total energy without the Coulomb contribution. Observe that the doorway molecular configurations correspond to the third snapshot from the left. Notice that the zero of all energies is taken at $d = 0$.

B. Open-Shell Parent Na_{18}^{2+}. Figure 2a displays the ATCOSM results for the symmetric channel $Na_{18}^{2+} \rightarrow 2Na_9^+$ (this channel is favored compared to that of the trimer, from both energetics and barrier considerations, see below), when, for illustrative purposes, the parent is assumed to be spherical at $d = 0$. The top panel of Figure 2a describes the evolution

of the single-particle spectra. The spherical ordering 1s, 1p, 1d, 2s, etc., for the parent at $d = 0$ is clearly discernible. With increasing separation distance, the levels exhibit several crossings, and, after the scission point, they naturally regroup to a new ordering associated with the spherical Na_9^+ products (at the end of the fission process, the levels are doubly degenerate compared to the initial configuration, since there are two Na_9^+ fragments). It is seen that the ATCOSM leads to an oscillator energy (i.e., the gap between two populated major shells exhibited at the right end of the figure) of 1.47 eV for each Na_9^+ fragment in agreement with the value expected from the one-center model [the 1s state of Na_9^+ lies at 2.21 eV; in the case of the initial spherical Na_{18}^{2+} ($d = 0$), the oscillator energy corresponding to the gap between major shells is 1.17 eV, and the corresponding 1s state lies at 1.75 eV].

From the middle panel of Figure 2a, we observe that the shell-correction (solid line) contributes a net gain in energy of about 1.6 eV upon dissociation into two Na_9^+ fragments. This gain is larger than the increase in energy (i.e., positive energy change) due to the surface term, which saturates at a value of about 1 eV after the scission point at $d \approx 23$ au. The total energy is displayed in the bottom panel of Figure 2a (solid line) along with the LDM barrier (dashed line). Even though distorted (when compared to the cases of Figure 1), the total barrier still exhibits a two-peak structure, the inner peak arising from the hump in the shell correction, and the outer peak arising from the point of saturation of the surface term (this last point coincides again with the scission point, as well as with the saddle of the LDM barrier). An inner local minimum is located at $d \approx 8$ au and corresponds to a compact prolate shape of the parent (see second drawing from the left at the top of Figure 2a), while a second deeper minimum appears at $d \approx 18$ au, corresponding to a superdeformed shape of a molecular configuration of two Na_9^+ clusters tied up together (preformation of fragments, see third drawing from the left at the top of Figure 2a). The inner barrier separating the compact prolate configuration from the superdeformed molecular configuration arises from the rearrangement of the single-particle levels during the transition from the initially assumed spherical Na_{18}^{2+} configuration to that of the supermolecule $Na_9^+ + Na_9^+$. We note that the barrier separating the molecular configuration from complete fission is very weak, being less than 0.1 eV.

The top dotted line at the bottom panel displays the total energy in the case when the Coulomb contribution is neglected. This curve mimics the total energy for the fusion of two neutral Na_8 clusters, namely, the total energy for the reaction $2Na_8 \rightarrow Na_{16}$. Overall, we find good agreement with a KS-LDA calculation for this fusion process (see Figure 1 of ref 23). We further note that the superdeformed minimum for the neutral Na_{16} cluster is deeper than that in the case of the doubly charged, Na_{18}^{2+} cluster. Naturally, this is due to the absence of the Coulomb term.

Figure 3a displays the ATCOSM results for the superasymmetric channel $Na_{18}^{2+} \rightarrow Na_{15}^+ + Na_3^+$, when again the parent is assumed to have a spherical configuration at $d = 0$ (see total energy denoted by the solid line in the bottom panel). It is observed that this channel exhibits a considerable barrier of about 0.9 eV, which is much higher than any of the barriers exhibited by the symmetric channel in Figure 2a. This barrier coincides with the hump in the shell-correction curve (the solid line at the middle panel) and thus is due to the rearrangement of the single-particle levels during the transition from the Na_{18}^{2+} parent to the $Na_{15}^+ + Na_3^+$ molecular configuration. An extremely weak outer hump at $d \approx 18$ au (associated again with the saturation of the surface term at the scission point) separates

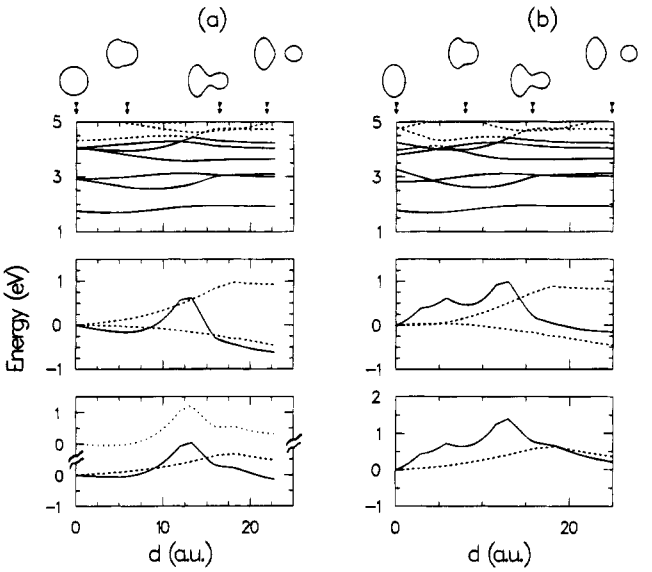

Figure 3. ATCOSM results for the superasymmetric channel $Na_{18}^{2+} \rightarrow Na_{15}^+ + Na_3^+$, when the initial parent shape is assumed (a) spherical and (b) oblate (with a shorter over longer axis ratio equal to 0.699). Panel distribution and other notations and conventions are the same as in Figure 1. The top dotted line in the bottom panel of (a) represents the total energy without the Coulomb contribution. Observe that the doorway molecular configurations correspond to the third snapshot from the left. Notice that the zero of all energies is taken at $d = 0$.

this molecular configuration from the eventual fission products. When the total energy is plotted without the Coulomb repulsion (dotted upper curve at bottom panel), the potential trough associated with the molecular configuration becomes slightly deeper, allowing for an easier identification of the doorway molecular configuration (see third drawing at the top of Figure 3a).

The natural way for producing experimentally the metastable Na_{18}^{2+} cluster is by ionization of the stable singly charged Na_{18}^+ cluster. Since this latter cluster contains 17 electrons and has a deformed oblate ground state,[6] it is not likely that the initial configuration of Na_{18}^{2+} will be spherical or prolate as was assumed for illustration purposes in Figures 2a and 3a. Most likely, the initial configuration for Na_{18}^{2+} will be that of the oblate Na_{18}^+. To study the effect that such an oblate initial configuration has on the fission barrier, we display in Figures 2b and 3b ATCOSM results for pathways for the two fission channels, starting from an oblate shape of Na_{18}^{2+}, proceeding to a compact prolate shape and then to full separation between the fragments via a superdeformed molecular configuration. We observe that additional potential humps (in the range 2 au $\leq d \leq$ 6 au), associated with the shape transition from the oblate to the compact prolate shape, develop for both channels. Concerning the total energies, the additional innermost humps result in the emergence of a significant fission barrier of about 0.52 eV for the favored symmetric channel (see $d \approx 5$ au in Figure 2b). In the case of the asymmetric channel, the fission barrier is now raised to about 1.35 eV, separating the oblate parent from the fission products (see $d \approx 13$ au in Figure 3b).

Conclusion

From the above analysis (Figures 1−3), we conclude that considerations of the energy pathways leading from the parent to preformation configurations (i.e., the inner-barrier hump or humps) together with the subsequent separation processes are most important for proper elucidation of the mechanisms of metal cluster fission processes. This corroborates earlier results obtained via ab initio molecular dynamics simulations[4,8,9]

pertaining to the energetics and dynamical evolution of fission processes, and emphasizes that focusing exclusively[11,13] on the separation process between the preformed state and the ultimate fission products provides a rather incomplete description of fission phenomena in metal clusters. It is anticipated that, with the use of emerging fast spectroscopies, experimental probing of the detailed dynamics of such fission processes could be achieved.

Acknowledgment. This research was supported by a grant from the U.S. Department of Energy (Grant No. FG05-86ER45234) and the AFOSR.

References and Notes

(1) Bréchignac, C.; Cahuzac, Ph.; Carlier, F.; de Frutos, M. *Phys. Rev. Lett.* **1990**, *64*, 2893; *Phys. Rev. B* **1994**, *49*, 2825.

(2) Bréchignac, C.; Cahuzac, Ph.; Carlier, F.; Leygnier, J.; Sarfati, A. *Phys. Rev. B* **1991**, *44*, 11386.

(3) Martin, T. P.; Näher, U.; Göhlich, H.; Lange, T. *Chem. Phys. Lett.* **1992**, *196*, 113; *Phys. Rev. Lett.* **1992**, *68*, 3416.

(4) Bréchignac, C.; Cahuzac, Ph.; Carlier, F.; de Frutos, M.; Barnett, R. N.; Landman, U. *Phys. Rev. Lett.* **1994**, *72*, 1636.

(5) Preston, M. A.; Bhaduri, R. K. *Structure of the nucleus*; Addison-Wesley: London, 1975.

(6) Yannouleas, C.; Landman, U. *Phys. Rev. B* **1995**, *51*, 1902.

(7) For a microscopic LDA foundation of the shell correction method (LDA-SCM) for metal clusters using the jellium approximation in connection with an extended Thomas–Fermi (ETF) LDA input density to a Harris-like functional, see refs 20–22. This LDA-SCM has been applied to multiply anionic metal clusters[20,21] and to multiply charged fullerenes (Yannouleas, C.; Landman, U. *Chem. Phys. Lett.* **1994**, *217*, 175).

(8) Yannouleas, C.; Barnett, R. N.; Landman, U. *Comments At. Mol. Phys.* **1995**, *31*, 445.

(9) Barnett, R. N.; Landman, U.; Rajagopal, G. *Phys. Rev. Lett.* **1991**, *67*, 3058.

(10) Maruhn, J.; Greiner, W. *Z. Phys.* **1972**, *251*, 431.

(11) Garcías, F.; Alonso, J. A.; Barranco, M.; López, J. M.; Mañanes, A.; Németh, J. *Z. Phys. D* **1994**, *31*, 275.

(12) Koizumi, H.; Sugano, S. *Phys. Rev. A* **1995**, *51*, R886.

(13) Rigo, A.; Garcías, F.; Alonso, J. A.; López, J. M.; Barranco, M.; Mañanes, A.; Németh J. In *Proceedings of ISSPIC7* (September 12–16, 1994, Kobe, Japan), to appear in *Surf. Sci. Rev. Lett.*

(14) The two-intersected-spheres jellium has also been used for describing the fusion of two neutral magic clusters (see ref 23).

(15) In this three-variables parametrization, the *B* parameter controls the necking-in, the *C* parameter controls the distance, and the α parameter controls the asymmetry, leaving no freedom for the shapes of the parent or the emerging fragments to be varied. In particular, both parents remain simultaneously either prolatelike or oblatelike, while final spherical shapes are excluded altogether. The weaknesses of the "funny hills" parametrization with respect to metal-cluster fission have been discussed in: Näher, U.; Frank, S.; Malinowski, N.; Zimmermann, U.; Martin, T. P. *Z. Phys. D* **1994**, *31*, 191.

(16) Mustafa, M. G.; Mosel, U.; Schmitt, H. W. *Phys. Rev. C* **1973**, *7*, 1519.

(17) *Handbook of mathematical functions*; Abramowitz, M.; Stegun, I. A., Eds.; Dover: New York, 1965.

(18) Strutinsky, V. M. *Nucl. Phys. A* **1967**, *95*, 420; *Nucl. Phys. A* **1968**, *122*, 1.

(19) Jennings, B. K. *Nucl. Phys. A* **1973**, *207*, 538. Jennings, B. K.; Bhadhuri, R. K.; Brack, M. *Phys. Rev. Lett.* **1975**, *34*, 228.

(20) Yannouleas, C.; Landman, U. *Phys. Rev. B* **1993**, *48*, 8376.

(21) Yannouleas, C.; Landman, U. *Chem. Phys. Lett.* **1993**, *210*, 437.

(22) Barnett, R. N.; Yannouleas, C.; Landman, U. *Z. Phys. D* **1993**, *26*, 119.

(23) Knospe, O.; Schmidt, R.; Engel, E.; Schmitt, U. R.; Dreizler, R. M.; Lutz, H. O. *Phys. Lett. A* **1993**, *183*, 332.

JP951572M